A STUDY OF THERMAL BEHAVIOR OF THE MACHINE TOOL SPINDLE

by

Aleksandar M. ŽIVKOVIĆ, Milan V. ZELJKOVIĆ*, Cvijetin D. MLADJENOVIĆ, Slobodan N. TABAKOVIĆ, Zoran Lj. MILOJEVIĆ, and Miodrag J. HADŽISTEVIĆ

Faculty of Technical Sciences, University of Novi Sad, Novi Sad, Serbia

Original scientific paper
https://doi.org/10.2298/TSCI180129118Z

The performances of high-speed machine tools depend not only on the speed, power, torque, dynamic and static stiffness, but also on the thermal behavior of the spindle. These parameters directly affect the productivity and quality of machining operations. This paper presents a 3-D finite element thermal model, which was based on the thermo mechanical bearing model and the numerical model of the spindle. Based on thermo mechanical analysis of bearings with angular contact, generated heat and thermal contact resistance are determined for each position of the ball. To provide the most accurate analysis possible in determining thermal contact resistance , bearings are divided into several zones based on the geometry of their cross-section. The aforementioned constraints have been applied to the 3-D FEM model which allowed for establishing temperature field distribution, and spindle thermal balance. In order to prove the efficacy of the proposed model, experimental measurements of spindle and bearing temperatures were done by using thermocouples and thermal imager.

Key words: *machine tool, spindle unit, rolling bearing, thermal model, temperature field, finite element*

Introduction

One of the main machine tool components affecting the accuracy and productivity of machining is the spindle unit. The heat generated in bearings and the motor are transferred through the spindle elements, causing linear, and non-linear thermal expansion. Non-uniform temperature distribution causes elastic thermal deformation of the spindle shaft, resulting in workpiece geometric and shape errors. It is essential to determine thermal sources, sinks, and temperature distribution of high speed spindle, in order to reduce and compensate for the thermal errors of both the spindle and the entire machine tool. Bossmanns and Tu [1, 2] built a thermal model based on the finite difference method (FDM) for analyzing motor-spindle affected by speed and preload. Their generated heat model is a function of speed and load, without considering the influence of generated heat change based on the rise in temperature. The research of non-linear thermal effects on high speed spindles via FDM was performed by Than and Huang [3]. Jedrzejewski *et al.* [4, 5] presented a hybrid model of high speed machining center which consisted of a headstock modeled by FEM and using tetrahedral elements, and axisymmetric spindle with bearings modeled via FDM using ring elements. Li and Shin [6] depicted an integrated thermodynamic model based on FEM, with the relation between the increase in

* Corresponding author, e-mail: milanz@uns.ac.rs

temperature and the stationary change in bearing stiffness by using 2-D axisymmetric elements. The FEM analyses for quasi static analysis of bearing parameters during contact period in referent temperature was performed by Mitrović *et al.* [7]. Grujičić *et al.* [8] considered the factors that influence heat generation within a ball bearing. The new equation and methodology for ball bearings' internal clearance determination, which could be used for eventual improvement of existing bearings' service life equations, was presented by Mišković *et al.* [9]. *Ma et al.* [10, 11] implemented a geometrical-mechanical-thermal model for determining thermal contact resistance in 3-D FEM thermal spindle model. In the aforementioned papers, heat generated in the bearing and thermal contact resistances are determined only when in stationary state. Also, the amount of heat generated in the bearing, the temperature, and thermal contact resistance of the bearing are considered uniform for all balls. Thermal contact resistance has formerly been determined on the basis of uniform internal geometry of the bearing. On the other hand, there is no consideration of the change in viscosity of the lubricant due to the change in bearing temperature. With the increase in temperature, there is an expansion of bearing and spindle elements, which causes the increase in contact load of the bearing, thus increasing the generated heat and changing the thermal contact resistance depending on the ball position. The change in bearing element dimensions due to thermal expansion is usually ignored in the analysis of thermal behavior of machine tool spindle. All these parameters can significantly affect the accuracy of the results when analyzing the thermal behavior of machine tool spindle. Thus, the temperature-dependant characteristics of the spindle-bearing system, which are often ignored in research, will be investigated in detail in this paper. In this study, the thermo mechanical model of the bearing and the 3-D finite element model of the spindle are used to determine the influences of non-linear thermal effects on the thermal behavior of the machine tool spindle. The thermo mechanical model of the bearing has been improved in several major aspects:

– The generated heat and thermal contact resistance are determined for each ball, *i. e.* depending on the ball angular positions.
– Thermal contact resistance is determined based on the variable dimensions of the bearing cross-section. The bearing is divided into three zones based on the change in its cross-section dimensions.
– When determining the heat generated on the bearing and thermal contact resistance, the change in bearing element dimensions due to thermal expansion, and the change in viscosity of the lubricant depending on the temperature are both considered.
– The heat transfer coefficient of the spindle's stationary surfaces is determined based on the experimental testing in concrete conditions, since it depends on the testing conditions as well as the geometry of machine tool spindles. In current research, this coefficient has been taken from paper [1].

The proposed model is applied in researching the spindle thermal characteristics with "O" bearing arrangement. Variable heat sources and heat transfer coefficients were used on the thermal model. The geometric parameters of the bearing, contact angle after preload, initial preload, contact forces, contact angles with raceways, and inertial forces are considered in non-stationary state for each angular position of the ball. Likewise, the heat generated on the bearing, as well as thermal contact resistance, are analyzed in non-stationary state. Based on the specific temperatures of the spindle, new dimensions of balls and raceways are established. Afterwards the contact forces contact angles, thermal contact resistance for each ball as a result of thermal expansion are determined. The process is reiterated until it reaches the stationary temperature state, as any changes after that become negligible.

Finally, in order to determine the efficacy of the proposed model, experimental measurements of spindle and bearing temperatures were performed using the thermocouple, infra-red thermometer, and thermal imager.

The thermal model of the high-speed spindle

For the high-speed spindle shown in fig.1, heat generated by bearings $H_1(t)$ i $H_2(t)$ is the main heat source that is considered in the paper. The conditions of heat transfer from the spindle and the boundary conditions of heat dissipation are also shown in fig. 1. They include: convection between the spindle shaft nose and ambient air (h_{fc}), convection of the air in the annular gap (h_{gap}) (*e. g.* between the spindle shaft and the housing, and spindle shaft and outer distance ring), the conduction from balls to the inner and outer raceways (R_b), conduction between the outer bearing ring and the housing ($R_{or\text{-}h}$), conduction between the inner bearing ring and the spindle shaft ($R_{ir\text{-}s}$), and free convection of ambient air around the stationary surfaces (h_{free}). Also, in the process of analysis the following hypotheses were defined, which do not affect the results:

– The spindle model is axisymmetrical and assumes a uniform clearance between the outer ring and the housing around the entire perimeter.
– Some small structures such as holes, nuts and other micro-structures are not considered due to their minimal influence on the simulation results.
– Heat-flow resistance due to lubrication between balls and raceways is not considered, due to the minimal amount of grease.
– The heat radiation is neglected because the temperature difference during the spindle rotation is small.

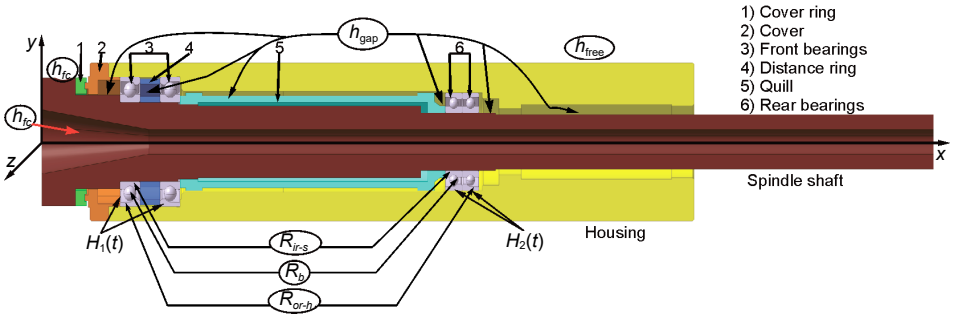

Figure 1. Thermal model of the high-speed spindle

The thermo mechanical model of the bearing

The mechanical and thermal processes in the bearing are connected. As the speed of bearing rotation increases, so does the heat generated on the contact surfaces of the bearing. On the other hand, variable heat sources and sinks cause complex thermal expansion, which creates additional thermal load.

Internal loading of the bearing

In ball bearings with angular contact the initial contact angle is defined by the line that goes through the contact points of balls and raceways, and the plane orthogonal to the bearing rotation axis. When there is no load, the raceway curvature centers, C_0 and C_{i1}, are located at the distance $A = Bd_b = (f_i + f_0 - 1)d_b$ as can be seen in fig. 2(a). Figure 2(b) shows the angular

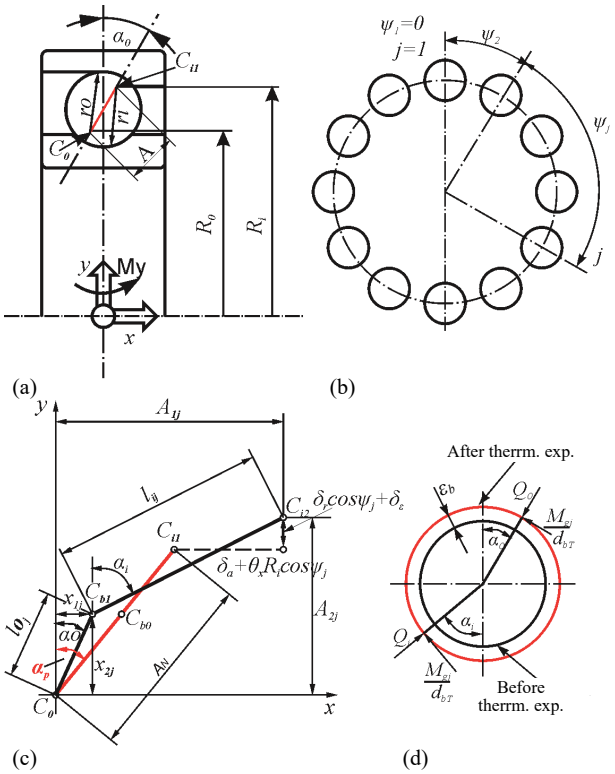

Figure 2. (a) Parameters of a ball bearing, (b) angular position of the ball, (c) position of raceway curvature centers, (d) ball loading at angular position ψ_j

position of the ball. The inertial forces, external load, and thermal load affecting the balls cause the change of contact angles with the outer and inner raceways. Due to the change in contact angle with the raceways the line of action between the raceway groove curvature centers will not be collinear with the distance between centers A_N as depicted in fig. 2(c). The inner raceway groove curvature center, C_{i1}, moves relatively compared to the center, C_o, which is fixed.

According to Pythagoras's theory the equation of kinematic constraints between balls and raceways in fig. 2(c) is [12, 13]:

$$\begin{aligned}&\left[A_N \sin\alpha_p + \delta_{ax} + \delta_{\varepsilon,ax} + \theta_y R_i \cos\left(\psi_j\right) - X_{1j}\right]^2 + \\ &+\left[A_N \cos\alpha_p + \delta_r \cos\left(\psi_j\right) + \delta_{\varepsilon,r} - X_{2j}\right]^2 + l_{ij}^2 = 0 \\ &X_{1j}^2 + X_{2j}^2 + l_{oj}^2 = 0\end{aligned} \tag{1}$$

Based on fig. 2(d) in accordance with Newton's 2nd law, for every ball the equation of forces in horizontal and vertical direction is defined:

$$\begin{aligned}&Q_{oj}\cos\alpha_{oj} - Q_{ij}\cos\alpha_{ij} - \frac{M_{gj}}{d_{bT}}\left(\sin\alpha_o - \sin\alpha_i\right) - F_{cj} = 0 \\ &Q_{oj}\sin\alpha_{oj} - Q_{ij}\sin\alpha_{ij} + \frac{M_{gj}}{d_{bT}}\left(\sin\alpha_o - \sin\alpha_i\right) = 0\end{aligned} \tag{2}$$

The method of determining gyroscopic moment and centrifugal force of a ball is shown in [14] in greater detail. The relation between local Hertz's contact forces $Q_{(j)}$ and deflection $\delta_{(j)}$ between ball and inner/outer raceway is defined:

$$Q_{m,j} = K_m \delta_{m,j}^{3/2}, \quad m = i,o, \quad j = 1,2....Z \tag{3}$$

Four parameters X_{1j}, X_{2j}, $\delta_{i(j)}$, $\delta_{o(j)}$ for each ball position were obtained by solving the non-linear relations of eqs. (1) and (2) in MATLAB using Newton-Raphson method, for the presupposed values of relative ring displacement (δ_{ax}, δ_r *i* θ_y). Permissible error in Newton-Raphson iterations is 10^{-10}.

The contact area with inner or outer raceway is defined:

$$A_{m,j} = a_{m,j} b_{m,j} \pi \tag{4}$$

where $a_{m,j}$ and $b_{m,j}$ represent the semi-major and semi-minor axis of the elliptical contact area and are defined for each position of the ball in accordance with [15]:

$$a_{m,j} = \sqrt[3]{\frac{6\kappa_m^2 R_{xy,m} Q_{m,j}}{\pi E''}}, \quad b_{m,j} = \sqrt[3]{\frac{6E'_m R_{xy,m} Q_{m,j}}{\pi \kappa_m E''}}, \quad m = i,o, \quad j = 1,2,...,Z \tag{5}$$

The heat generation of ball bearing

The generated heat of the bearing is created by three types of friction moment: torque due to applied load, torque due to viscosity of lubricant and spinning friction moment. Therefore, the friction torque due to applied load and due to viscosity of lubricant at each inner and outer contact with the raceway is formulated [13]:

$$M_{1m,j} = \left\{ f_1 \left(\frac{Q_{m,j}}{Q_{m(\max)}} \right)^{1/3} Q_{m,j} d_{bT} + 10^{-7} f_0 \left(\nu_o n \right)^{2/3} d_{mT}{}^3 \right\}, \quad m = i,o \; j = 1,2...Z \tag{6}$$

For the bearing SKF7011 CDGA HC/P4 which is lubricated by the SKF LGLT 2 grease the relation viscosity-temperature is given in tab. 1. The third component of heat generation within the bearing is the spinning friction moment generated by the spinning at the contact area of the balls and raceways. The spinning friction moment for every contact with the inner and outer raceway can be obtained [14]:

Table 1. The grease viscosity-temperature relationship

Temperature [°C]	25	40	60
Kinematics viscosity [mm^2s^{-1}]	30	18	11

$$M_{S,m,j} = \frac{3\mu Q_{m,j} a_{m,j} E^{'}}{8}, \quad m = i,o, \quad j = 1,2...Z \tag{7}$$

The heat generated in the contact zone for each ball:

$$H_{m,j} = \omega_b M_{1m,j} + \omega_{s,m,j} M_{S,m,j}, \quad m = i,j, \quad j = 1,2...Z \tag{8}$$

In fig. 3(a) the heat generated based on the position of the balls for the spindle speed of 9000 rpm is depicted, while affected by preload and external radial load on the bearing. Total generated heat on front and rear bearings is shown in fig. 3(b). Due to the influence of inertial forces, the contact angle and the contact load with the outer raceway are increased, which leads to an increase in heat generated on the outer raceway, versus the inner one. Thus, the difference

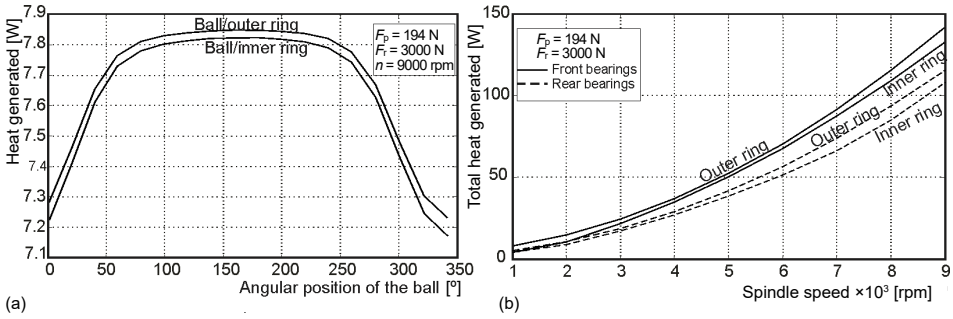

Figure 3. (a) Heat generated in the front bearings depends on the angular position of the balls and (b) total generated heat in front and rear bearings

in heat generated between the raceways, and the difference in heat generated based on the ball position are purely the consequences of bearing contact load and thermal expansion of the bearing rings and balls.

The mechanisms of heat transfer through the bearing

This paper presupposes that the mechanisms of heat transfer through the bearing are: the conduction between the balls and the raceways, fig. 4(a), the conduction between the outer ring and housing, fig. 4(b) and the conduction between spindle shaft and the inner ring, fig. 4(c).

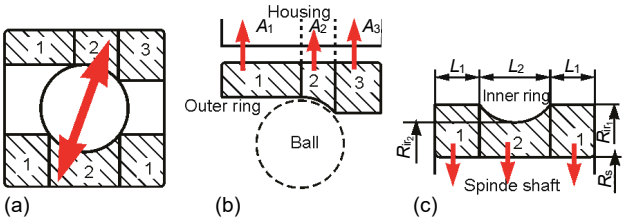

Figure 4. Heat transfer through bearings: (a) the conduction between the balls and the raceways, (b) the conduction between the outer ring and housing, (c) the conduction between spindle shaft and the inner ring

Conduction between balls and rings

Thermal contact resistance depends on the shape and size of the contact area, and it is connected to the bearing geometry and the contact forces in the bearing. According to [1, 14, 15] for those cases where the balls and rings are not made of the same material, thermal contact resistance for each ball:

$$R_{b(m,j)} = \frac{1}{2\pi a_{m,j}\lambda_b}\psi\left(e,\frac{\pi}{2}\right) + \frac{1}{2\pi a_{m,j}\lambda_{\text{ring}}}\psi\left(e,\frac{\pi}{2}\right), \quad m = i,o, \quad j = 1,2,....,Z \tag{9}$$

where λ_b and λ_{ring} are thermal conductivity of the balls and rings, respectively, and $\psi(e, \pi/2)$ is a geometrical factor dependent on the size of contact area between balls and raceways. It is defined:

$$\psi\left(e,\frac{\pi}{2}\right) = \int_0^{\pi/2} \frac{\mathrm{d}\theta}{\sqrt{1-k_{m,j}^2\sin^2\theta}}, \quad k_{m,j} = 1 - \frac{b^2{}_{m,j}}{a^2{}_{m,j}} \tag{10}$$

where *a, b* are the elliptic contact axes as defined in relation (5).

Thermal contact resistance for each ball position in the function of preload is shown in fig. 5. In fig. 5(a), the change in thermal contact resistance, depending on the position of the ball under constant preload with external radial load, is shown. The change in thermal contact

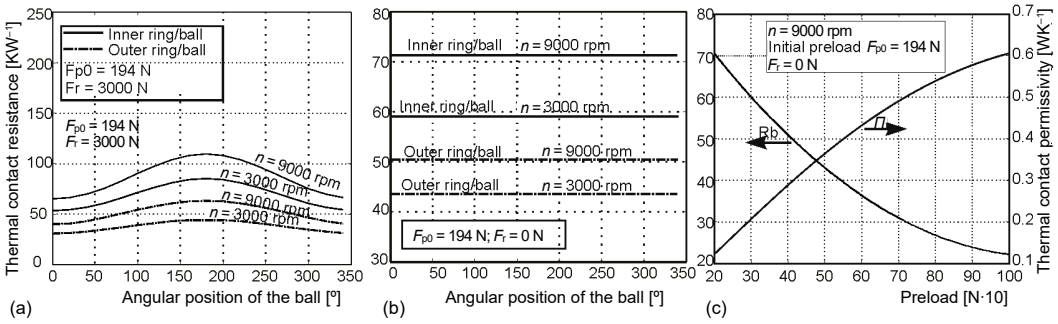

Figure 5. Thermal contact resistance of the front bearings

resistance based on preload without any external radial load can be seen in fig. 5(b) and 5(c). Based on the aforementioned figures, it can be seen that thermal contact resistance is not uniform when there is radial load, but is maximal on the balls with maximum contact loads. When there is no external radial load, thermal resistance is the same for all balls, fig. 5(b) and decreases with the increase in preload, while thermal permissivity, Π, rises since it is inversely proportional to thermal resistance, fig. 5(c) which is in alignment with [16] and Bossmanns and Tu [1].

Conduction between outer ring and housing

Heat conduction between the outer ring and housing is non-uniform for the entire width of bearing, since ring thickness is not constant for the width. Based on that, the outer ring is divided in three parts as depicted in fig. 4(b). Thermal contact resistance between the outer ring and the housing is defined in accordance with [3], while taking into consideration the change in outer ring cross-section:

$$R_{or-h} = \frac{h_{\text{ring},(i)}}{\lambda_{\text{ring}} A_{(i)}} + \frac{h_{\text{gap}} - (T_{\text{ring}} - T_h)\alpha_{te} r_h}{\lambda_{\text{air}} A_{(i)}} \tag{11}$$

where $h_{\text{ring}(i)}$ is the ring thickness for the specific cross-section (i = 1,2,3), $A_{(i)}$ – the contact area of the outer ring and the housing for a specific cross-section, α_{ts} – the thermal expansion coefficient, and r_h – the internal radius of the housing. Thermal permissivity between the outer ring and the housing is inverse to the thermal contact resistance ($\Pi = 1/R_{or\text{-}h}$) and it depends on their temperature difference. Figure 6 shows the change in thermal permissivity depending on the temperature difference for the examined spindle.

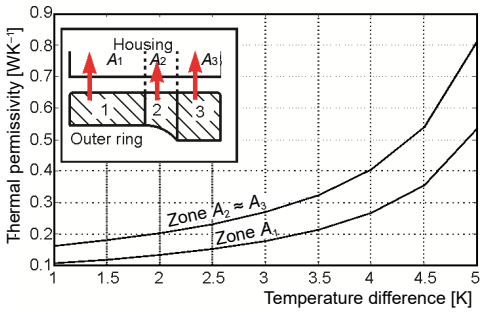

Figure 6. Thermal permissivity for conduction between outer ring and housing as a function of ΔT

Conduction between the inner ring and spindle shaft

As in the previous case, because of the change in inner ring thickness in width, it is divided into two parts as is shown in fig. 4(c). Heat resistance, $R_{ir\text{-}s}$, between the inner ring and the spindle shaft is determined by using the relation for cylinder heat resistance [17]:

$$R_{ir-s} = \frac{\ln(R_{ir(i)}/R_s)}{2\pi L_{(i)}\lambda_{\text{ring}}} \tag{12}$$

where $R_{ir(i)}$ $(i = 1,2)$ and R_s are the inner section radii which are observed in the inner bearing ring according to fig. 4(c), and $L_{(i)}$ is the length according to the inner section, fig. 4(c). Heat conductivity, λ, for steel is 46.6 W/mK and it is valid for 20-200 °C [18]. The values of the conduction between the inner ring and spindle shaft are listed in tab. 2.

Table 2. The TCR of the conduction between the inner ring and spindle shaft

Zone	Thermal contact resistance [m^2KW^{-1}]
Zone 1	3231.5
Zone 2	3301.6

Mechanisms heat transfer from spindle

The spindle in rotation produces relative movement between the surface and the surrounding air, thus creating forced convection. Mechanisms heat transfer in the high-speed spindle includes force convections at the small annular gap, force convections of the rotation bodies, and free convection on the stationary surfaces. The heat transfer mechanisms of the spindle that are considered here are shown in fig. 2.

Heat transfer coefficient for force convection can be established as [17]:

$$h_i = \frac{\text{Nu}\,\lambda_{\text{air}}}{d_j}, \quad i = fc, \quad \text{gap}, \quad j = d, d_e, \text{gap} \tag{13}$$

where λ_{air} is the heat conductivity of air, Nu – the Nusselt's number, and d_j – the diameter of the flow cross-section of a tube, as shown in fig. 1. In case of annular gap of the spindle, d_j changes to the size of gap.

Force convections of the rotation bodies. For the laminar air-flow around the rotating spindle the Nusselt's number is determined [19]:

$$\text{Nu} = 0.118\,\text{Re}^{0,66}$$
$$\text{Re} = \frac{\omega_s d_j^2}{\nu_{\text{air}}}, \quad \text{Re} < 4.3\cdot 10^5 \tag{14}$$

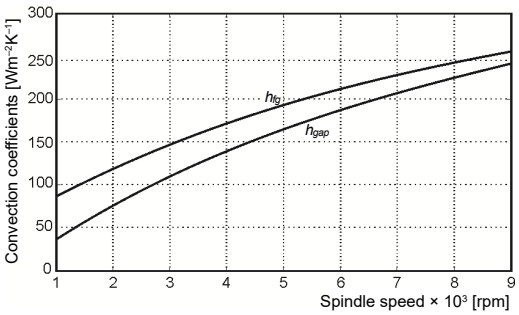

Figure 7. Variations of $h_{\text{frot. body}}$ h_{annulus}, with spindle speed

Figure 7 shows force convections variations of the rotation bodies and force convections in the annular gap in according with the fig. 1, with respect to the specific rotation speed of the spindle.

Free convection on the stationary surfaces. In this paper the housing temperature measurement was taken for different spindle rotation speeds. The measurements were done until the stationary state was reached, after which the spindle was shut down and the cooling temperatures of the housing were monitored. Based on the curve of the cooling, via the analytic method through the use of relation (15) the free convection coefficient of the housing was established as shown in fig. 8.

$$m_h c_h \frac{\partial T_{(t)}}{\partial t} = h_{(t)\text{free}} \left[T_h(t,z) - T_0 \right] A(z) \quad (15)$$

In these experiments the free convection coefficient is 17.48 W/m^{2}K, for spindle speed n = 3000 rpm, which is in alignment with [20], *i. e.* 32.12 and 38.84 W/m^{2}K for spindle speed n = 6000 rpm and n = 9000 rpm, respectively.

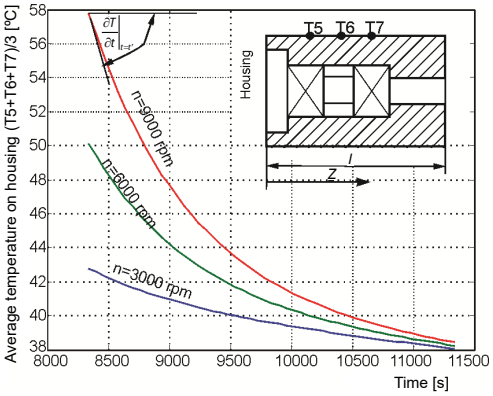

Figure 8. Estimation of the free convection coefficient for the housing

The FEM thermal model

In defining the thermal model of the spindle, *i. e.*, the spindle shaft, bearings (rings and balls), and the housing, the hexahedral element SOLID 90 was used to mesh solid structure. In order to improve the accuracy and speed at the same time, elements with higher temperature, *i. e.* the raceways and balls, are meshed in a more refined manner. Model consists of 125353 solid elements and 211303 nodes in total. The finite elements CONTA174 and TARGET170 were used to simulate contact joints. To simulate contact joints, contact pairs were created at the joints, and the real constant (TTC) was defined, *i. e.*, the thermal contact conductivity for each ball, as well as for each contact between the outer ring/housing and inner ring/spindle shaft according to fig. 4. Because of the spindle symmetry only a half of the 3-D model was considered, as shown in fig. 9. Based on the first law of thermodynamics on energy conservation, the transient heat transfer model for the 3-D model is derived:

$$\rho c_p \frac{\partial T_{(x,y,z,t)}}{\partial t} = \frac{\partial}{\partial x}\left[\lambda_{(T)} \frac{\partial T_{(x,y,z,t)}}{\partial x} \right] + \frac{\partial}{\partial y}\left[\lambda_{(T)} \frac{\partial T_{(x,y,z,t)}}{\partial y} \right] + \frac{\partial}{\partial z}\left[\lambda_{(T)} \frac{\partial T_{(x,y,z,t)}}{\partial z} \right] + H_1(t) + H_2(t) \quad (16)$$

where $T = T_{(x,y,z,t)}$ is the temperature of the each element, t [s] – the time, To completely construct the 3-D finit element model in the *ANSYS Workbranch 18-Academic*, all convection and contact conductance coefficients must be computed using aforementioned relations and set up in the model.

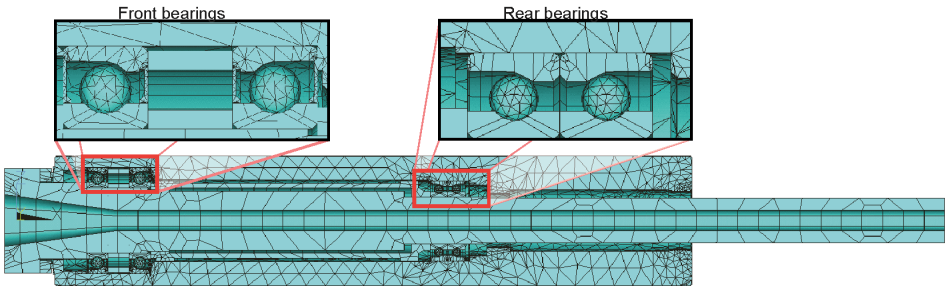

Figure 9. The 3-D finit element model of the spindle unit

Experimental set-up

In order to validate simulation results, an experimental apparatus has been established to measure temperatures shown in fig. 10. The spindle is driven by motor, which has 9000 rpm maximum speed, through belt transmission. The driving motor – 2 is, by belt transmission – 3, connected to spindle shaft – 1 and frequency regulator – 4, which allows for the desired rpm. To measure the temperature of the spindle, thermocouples, infrared thermometer, and thermal imager have been used. Two K-type thermocouples (T1, T2) have been placed through the housing – 5 on front bearings' outer rings, fig. 10(b). Additional three K-type thermocouples (T5, T6, T7) have been placed on the housing – 5, where the spindle support is located (near the front bearing), fig. 10(a). The accuracy of measurement of the K-type thermocouple according to the standard BS1041-4 is in the range of ±3 °C between 0° C and 400 °C. The temperatures obtained from these thermocouples were collected by an acquisition system NI USB 6281 and then sent back to a computer for processing and monitoring results for every one second. The output from the acquisition system is continuously monitored and analyzed in MATLAB software. Infrared thermometer – 6 has been used to record temperature (T4) at the inner tapered surface of the spindle shaft, fig.10(b). The accuracy of measurement of the infrared thermometer was ±2 °C between –40° C and 500 °C. To record the distribution of temperature fields, monitor the temperatures of the entire experimental rig, and record temperature (T3) at spindle nose, as well as to control the thermocouples, the Thermo Pro^{TP} TP8S thermal imager – 7 has been used. The accuracy of measurement of the Thermo Pro^{TP} TP8S thermal imager was ±1 °C between –20° C and 250 °C. The spindle, fig. 10(b) is mounted on the experimental test rig with a headstock – 8, and it is projected to work in a span of 0-9000 rpm. The spindle is supported in the front with two bearings in a "0" arrangement (SKF 7011 CDGA/HC P4.), and in the rear with two bearings in a "0" arrangement (SKF 7008 CDGA/HC P4.). All the bearings are with lock-ring preload. The initial preload is 194 N.

Results and discussion

The analysis of the spindle's thermal characteristics includes the stationary and non-stationary state, as well as the analysis of the heat balance. For the stationary and non-stationary analysis, the temperatures measured in different measuring points, fig. 10, were compared to the predicted temperatures received from the mathematical model for different spindle speed. Also, thermal field distribution that was devised in the mathematical model was compared to the actual thermal distribution field as measured by thermal imager.

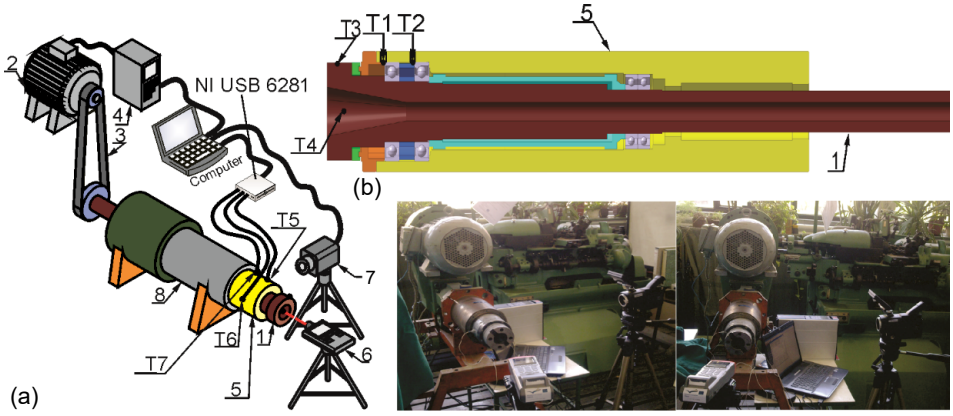

Figure 10. A schematic; (a) of the experimental rig and (b) of the spindle

Steady-state analysis

Figure 11(a) predicts the temperature distribution of the spindle for rotation speed of 9000 rpm and reference temperature of 22 °C. In fig. 11(b), the comparison between the distribution of temperature fields, which were obtained experimentally by using the thermal imager and simulation, is shown. According to fig. 11(a) it can be seen that the temperatures on the front bearings and around front bearings are higher than the temperatures of the other spindle elements, and that temperature field distribution is not uniform for the spindle and housing. The rise in temperature of the bearing is caused by the friction of balls and rings. Thus, the heat accumulated in the bearing's transfers to the spindle and housing, with the larger part of it being on the housing. The maximum differences from 2 to 5 °C in stationary state, depending on the measurement points, are acceptable.

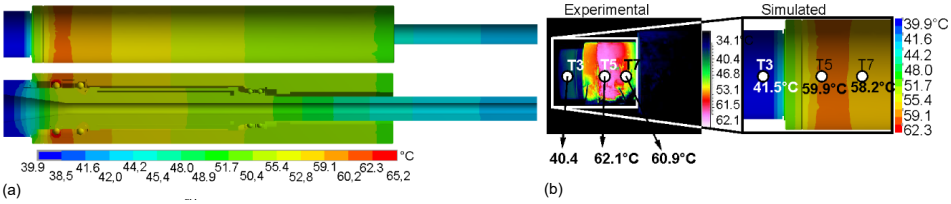

Figure 11. Temperature distribution of the spindle for 9000 rpm; (a) Simulated and (b) experimental via thermal imager (*for color image see journal web site*)

Transient state analysis

Figure 12 shows the comparison between measured and simulated temperatures on the front bearings during time. In fig. 13 there are the comparisons between the measured and predicted temperature histories of the housing and spindle nose. The temperatures of the front bearings from the very start rise sharply at the early stage, and then gradually increase until reaching the final temperature, when the amount of heat generation is in balance with the heat dissipation into the ambient air. It takes about 60 min for the front bearings to reach a thermal equilibrium state. In fact, the rotational speed of the spindle has a significant effect on the thermal balance, because of the dependence of the heat generation of the bearings on the spindle speed. The higher the rotational speed of the spindle, the shorter it will take to reach the stationary state. According to fig. 13(c), there is a visible short rise of spindle nose temperature as observed in both simulation and experiments, which is produced due to the equalization of higher core temperatures that transfer through the spindle after it is shut off. In the first-time stage, the temperature on the housing increased faster than that of the shaft and more slowly than the temperature on the bearings. Through these findings, the history of temperature distribution on the spindle-bearing system can be learned, and a suitable cooling system can be designed to minimize thermal expansion.

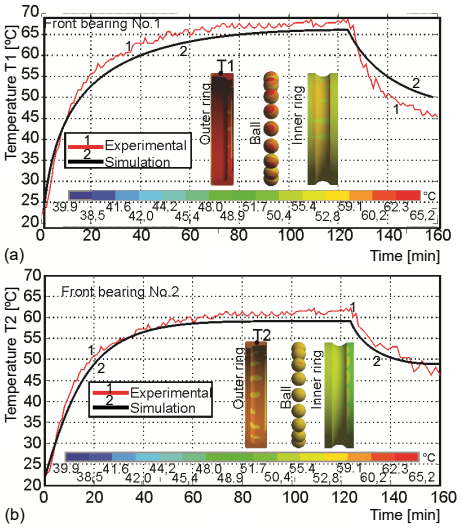

Figure 12. The temperature changes during time at the front bearing; (a) No. 1, (b) No. 2 (*for color image see journal web site*)

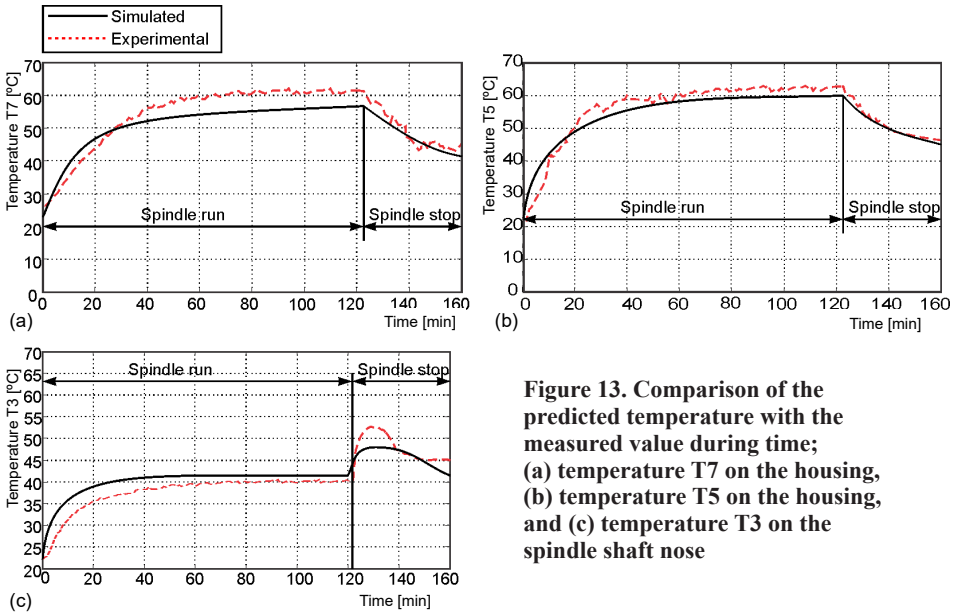

Figure 13. Comparison of the predicted temperature with the measured value during time; (a) temperature T7 on the housing, (b) temperature T5 on the housing, and (c) temperature T3 on the spindle shaft nose

The analysis of power balance

The thermal balance procedure determines internal heat generation and heat transfer coefficients as functions of spindle speed. Independently from the calculation of heat sources, internal heat transfer is calculated from the predicted temperature field. All heat sources and heat sinks are finally added up, and the assumptions are considered valid when the power balance amounts to zero for all combinations of spindle speeds. Internal power flow has been analyzed through simulation and from experiments. The total amount of heat generated is 530 W as a consequence of friction in all four bearings. The front bearings produce about 292 W, while the rear bearings about 238 W.

The heat removed by the heat sinks include: 147.4 W from convection of the annular gap and around spindle nose into air, 289.5 W absorbed by the ambient air around the stationary surfaces, 88,1 W conducted through the spindle and housing. The total is 525 W. Compared to the input power, there is an error of 5 W.

Conclusions

A comprehensive method for determining temperature fields and considering a nonlinear thermal effect on high speed spindle is presented in this paper. Present model can be separated into two sub-models: the thermo mechanical bearing model and the thermal model of the spindle. Additionally, it is related to the bearing model through the generated heat, convective coefficient and thermal contact resistance. On one hand, the presented bearing model can be used for non-stationary simulation of the interaction of the internal bearing behavior, and on the other hand, for heat transfer and structural deformation of the spindle elements. The bearing model can be used for any type of bearing with angular contact and lock-ring preload. The temperature field distribution of the high-speed spindle system was calculated. As temperature changed, the variability in thermal contact resistance between two parts, such as balls/rings, outer ring/housing, and inner ring/shaft, was also noted. The temperature distribution in the spindle-bearing system was presented and found consistent with experimental results. The

maximum difference of 2 to 5 °C (about 3 to 5%) in stationary state, depending on the measurement points, is acceptable for the machine tool spindle analysis, especially since the suggested model assumes a uniform clearance between the outer ring and the housing around the entire perimeter. Changes in clearance affect the accuracy of several parameters, such as contact load, contact resistance, and generated heat in the bearing. On the other hand, any deviations of the numerical and experimental results are the consequence of errors in numeric mathematics of the 3-D model being discretized, the assumptions used in the mathematical model, and measurement accuracy. The distribution of temperature field of the spindle system was characterized according to the simulation results. Although the model was developed for the analysis of a high-speed spindle system, it can also be used for thermal analysis of various machining systems. Finally, improving the analysis of thermal spindle behavior made the model more accurate and predictive.

Acknowledgment

In this paper, some results of the project *Contemporary approaches to the development of special solutions related to bearing supports in mechanical engineering and medical prosthetics*–TR 35025, carried out by the Faculty of Technical Sciences, University of Novi Sad, Serbia, are presented. The project is supported by the Ministry of Science and Technological Development of the Republic of Serbia.

Nomenclature

A – distance between raceway groove curvature centers, [mm]
A_N – distance between raceway groove curvature centers after preload, [mm]
A1, A2, A3 – areas of the characteristic cross-sections (1, 2, 3) on the bearing ring according with fig. 4, [mm^2]
a – semi-major axis of the contact area, [mm]
b – semi-minor axis of the contact area [mm]
C_0 – outer raceway groove curvature center, [mm]
C_{b0} – ball center, initial position, [mm]
C_{b1} – ball center, final position, [mm]
C_{i1} – initial position, inner raceway groove curvature center, [mm]
C_{i2} – final position, inner raceway groove curvature center, [mm]
d_b – diameter of the balls, [mm]
d_{bT} – diameter of the balls after thermal expansion, [mm]
d_m – bearing pitch diameter, [mm]
E' – compl. ellip. integral of the second kind, [–]
E – moduls of elasticity, [Nmm^{-2}]
E'' – $2/(1-\eta_{ring}^2)/E_{ring} + (1-\eta_{ball}^2)/E_{ball}$, [–]
F – external load, [N]
F_c – centrifugal force, [N]
F_p – initial preload, [N]
f – r/d_b, [–]
H – heat generated, [W]
K – load-deflection constant, [–]
L.1, L.2, L.3 – lenght of the characteristic cross-sections (1, 2, 3) on the bearing ring according with fig. 4, [mm]
M – friction torque, [Nmm]
M_g – Gyroscopic moment, [Nmm]
Q – contact force, [N]
R – radius of the raceways, [mm]
R_x,R_y – effective radius, [mm]
$R_{xy,m}$ – $R_{x,m}R_{y,m}/(R_{x,m}+R_{y,m})$, [mm]
r – groove curvature radius, [mm]
Z – number of the ball, [–]
κ_m – $1.0339(R_{y,m}/R_{x,m})^{0.636}$, [–]

Greek symbols

α – contact angle, [°]
α_p – contact angle after preload, [°]
δ – deformation or deflection, [mm]
δ_ε – thermal expansion [mm]
ε_b – thermal expansion of the ball [mm]
η – Poisson coefficient, [–]
μ – friction coefficient [-]
ν – kinematic viscosity of lubricate [mm^{2}s^{-1}]
ψ – angular position of ball [°]
ω_b – angular velocity of the ball, [rads^{-1}]
ω_s – spin velocity [rads^{-1}]

Subscripts

ax – axial direction
i – refer to inner raceway
o – refer to outer raceway
r – radial direction

References

[1] Bossmanns, B., Tu, J. F., Thermal Model for High Speed Motorized Spindles, *International Journal of Machine Tools and Manufacture*, *39* (1999), 9, pp. 1345-1366
[2] Bossmanns, B., Tu, J. F., A Power Flow Model for High Speed Motorized Spindles – Heat Generation Characterization, *Journal of Manufacturing Science and Engineering, Transactions of the ASME*, *123* (2001), 3, pp. 494-505
[3] Than, V.-T., Huang, J. N., Nonlinear Thermal Effects on High-Speed Spindle Bearings Subjected to Preload, *Tribology International, 96* (2016), Apr., pp. 361-372
[4] Jedrzejewski, J., *et al.*, Hybrid Model of High Speed Machining Centre Headstock, *CIRP Annals - Manufacturing Technology, 53* (2004), 1, pp. 285-288
[5] Jedrzejewski, J., *et al.*, High-Speed Precise Machine Tools Spindle Units Improving, *Journal of Materials Processing Technology*, *162-163* (2005), May, pp. 615-621
[6] Li, H., Shin, Y. C., Integrated Dynamic Thermo-Mechanical Modeling of High Speed Spindles, Part 1: Model Development, *Journal of Manufacturing Science and Engineering, Transactions of the ASME*, *126* (2004), 1, pp. 148-158
[7] Mitrović, R. M., *et al.*, Effects of Operation Temperature on Thermal Expansion and Main Parameters of Radial Ball Bearings, *Thermal Science*, *19* (2015), 5, pp. 1835-1844
[8] Grujičić, R. N., *et al.*, The Analysis of Impact of Intensity of Contact Load and Angular Shaft Speed on the Heat Generation Within Radial Ball Bearing, *Thermal Science*, *20* (2016), 5, pp. 1765-1776
[9] Mišković, Ž. Z., *et al.*, Analysis of Grease Contamination Influence on the Internal Radial Clearance of Ball Bearings by Thermographic Inspection, *Thermal Science*, 20 (2016), 1, pp. 255-265
[10] Ma, C., *et al.*, Thermal Characteristics Analysis and Experimental Study on the High-Speed Spindle System, *The International Journal of Advanced Manufacturing Technology*, *79* (2015), 1-4, pp. 469-489
[11] Ma, C., *et al.*, Simulation and Experimental Study on the Thermally Induced Deformations of High-Speed Spindle System, *Applied Thermal Engineering*, *86* (2015), July, pp. 251-268
[12] Živković, A., Computer and Experimental Analysis of Behavior Ball Bearings for Special Applications, Ph. D. thesis, University of Novi Sad, Faculty of Technical Science, Novi Sad, Serbia, 2013
[13] Živković, A., *et al.*, Mathematical Modeling and Experimental Testing of High-Speed Spindle Behavior, *The International Journal of Advanced Manufacturing Technology*, *77* (2015), 5-8, pp. 1071-1086
[14] Harris, T. A., Michael, N. K., *Rolling Bearing Analysis: Advanced Concepts of Bearing Technology*, Taylor & Francis Group, Oxford, UK, 2007
[15] Harris, T. A., Michael, N. K., *Rolling Bearing Analysis: Essential Concepts of Bearing Technology*, Taylor & Francis Group, Oxford, UK, 2007
[16] Nakajima, K., Thermal Contact Resistance between Balls and Rings of a Bearing Under Axial, Radial, and Combined Loads, *Journal of Thermophysics and Heat Transfer*, *9* (1995), 1, pp. 88-95
[17] Incropera, F. P., *et al.*, *Fundamentals of Heat and Mass Transfer*, John Wiley and Sons, New York, USA, 2011
[18] Yovanovich, M. M., Thermal Constriction Resistance between Contacting Metallic Paraboloids: Application to Instrument Bearings, *AIAA Progress in Astronautics and Aeronautics: Heat Transfer and Spacecraft Control*, *24* (1971), pp. 337-358
[19] Zhang, J., *et al.*, A Method for Thermal Performance Modeling and Simulation of Machine Tools, *The International Journal of Advanced Manufacturing Technology*, *68* (2013), 5-8, pp. 1517-1527
[20] Takabi, J., *et al.*, Experimental Testing and Thermal Analysis of Ball Bearings, *Tribology International*, *60* (2013), Apr., pp. 93-103

Paper submitted: January 29, 2018
Paper revised: March 19, 2018
Paper accepted: March 24, 2018